

Cite this article as: Mei Jinna, Wu Tiandong, Wei Na, et al. Microstructure Evolution of FeCrNiMn Duplex High Entropy Alloys During High-Temperature Compression[J]. Rare Metal Materials and Engineering, 2022, 51(12): 4496-4501.

ARTICLE

Microstructure Evolution of FeCrNiMn Duplex High Entropy Alloys During High-Temperature Compression

Mei Jinna¹, Wu Tiandong^{2,3}, Wei Na^{2,3}, Cai Zhen¹, Xue Xiangyi^{2,3}

¹Suzhou Nuclear Power Research Institute, Suzhou 215004, China; ²Xi'an Chao Jing Technology Co., Ltd, Xi'an 710200, China; ³Shaanxi Key Laboratory of Advanced Metal Structural Materials Precision Thermoforming, Xi'an 710200, China

Abstract: To investigate the microstructure evolution during high-temperature deformation of the duplex high entropy alloys (HEAs), compression tests were performed at temperatures from 900 °C to 1050 °C with different strain rates. Four typical flow curves were selected and the corresponding microstructures were analyzed to investigate the dynamic recrystallization (DRX) and texture evolution of the duplex HEAs. The results show that the flow curves are totally different for samples deformed at the strain rate of 0.1 and 0.01 s⁻¹. The difference of mechanical flow curves is correlated with the DRX and texture evolution process. Two-component textures combining the <110> and <100> components are obtained after compression at 1050 °C and 0.1 s⁻¹. It is attributed to the dominance of diffusion-controlled solute drag at high temperature. Moreover, the effect of bcc phase relies on interphase boundary and strain heterogeneity around these particles, since no phase transformation occurs and most of the strain is accommodated by fcc phase.

Key words: high entropy alloy; microstructure evolution; high-temperature deformation; flow curves

High entropy alloys (HEAs) have attracted extensive attention since firstly proposed by Yeh ^[1] due to the excellent properties, such as high strength, high temperature softening resistance, irradiation resistance and wear resistance^[2-4]. The multi-principal element alloys possess extraordinary mechanical properties because of the well-known four “core effects”: high configurational entropy, lattice distortion, sluggish diffusion and cocktail effect ^[5]. HEAs are considered to be the most promising new high-performance structural materials and have become the research hotspot in the field of solid mechanics and materials science.

The early work on HEAs mainly focused on single phase face-centred cubic (fcc) and body-centred cubic (bcc) materials^[6,7]. However, in many cases fcc HEAs generally show high plasticity but insufficient strength, while bcc HEAs exhibit poor ductility despite high strength^[8,9]. To overcome this drawback, the development of multi-phase, especially fcc plus bcc duplex HEAs was encouraged^[10,11]. Although the duplex HEAs offer a good balance between strength and ductility, systematic research on the complex deformation

mechanisms and structure evolution during high-temperature deformation is rarely performed. It has been investigated that solution hardening and stacking fault energy might change the dominant recrystallization mechanism of cubic alloys^[12,13]. The fcc and bcc phases normally have totally different strength and stacking fault energy, and thus may exhibit a complex deformation and restoration behavior. Lee^[14] and Kim^[15] have demonstrated fast recrystallization kinetics in duplex HEAs because of particle stimulated nucleation provided by bcc particles. Haghdad et al^[16,17] have systematically studied the dynamic recrystallization (DRX) in duplex AlXCoCrFeNi alloy. Despite these work, further studies of the microstructural evolution of duplex HEAs need to be performed.

In this work, high-temperature compression tests of the FeCrNiMn duplex alloy were conducted under various deformation conditions. Four distinct flow curves were selected, and the corresponding microstructures were analyzed by electron back-scattered diffraction (EBSD) to investigate the DRX and texture evolution of the duplex alloy.

Received date: December 12, 2021

Foundation item: Natural Science Foundation of Jiangsu Province (BK2018021)

Corresponding author: Wei Na, Master, Shaanxi Key Laboratory of Advanced Metal Structural Materials Precision Thermoforming, Xi'an Super Crystal Sci-Tech Development Co., Ltd, Xi'an 710200, P. R. China, E-mail: weina@super-c.com.cn

Copyright © 2022, Northwest Institute for Nonferrous Metal Research. Published by Science Press. All rights reserved.

1 Experiment

The FeCrNiMn alloy used in this study was vacuum arc remelted three times to ensure a well-distributed composition. A cylindrical rod with dimensions of $\Phi 54 \text{ mm} \times 110 \text{ mm}$ was cut from the ingot and forged at $1050 \text{ }^\circ\text{C}$. Then a heat treatment under $1200 \text{ }^\circ\text{C}/1 \text{ h}$ followed by air cooling was performed to obtain the duplex microstructure. The samples for high-temperature compression were wire cut from the heat treated forging billet. Then the samples were turned to a size of $\Phi 8 \text{ mm} \times 12 \text{ mm}$. The compression tests were performed on a Thermecmaster-Z thermo-mechanical testing machine at temperatures from $900 \text{ }^\circ\text{C}$ to $1050 \text{ }^\circ\text{C}$ with different strain rates. The strain and stress data were recorded during the whole compression process. The samples were air quenched immediately after compression tests to preserve the microstructure at high temperatures.

After the compression tests, the samples were cut along the compression direction and electro-polished for microstructural analysis. The chemical compositions of different phases in the annealed samples were analyzed by an energy dispersive spectroscopy (EDS). The microstructures of the deformed samples were analyzed by a Zeiss-Sigma500 scanning electron microscope (SEM) operated at 20 kV . EBSD was conducted at step sizes of 0.5 and $0.15 \text{ }\mu\text{m}$ to study the microstructures.

2 Results and Discussion

2.1 Initial microstructures

The SEM image and EBSD maps of the FeCrNiMn alloy used for high-temperature compression are shown in Fig. 1. The raw material exhibits a duplex structure. It consists of

about 96vol% equiaxed fcc grains and 4vol% bcc particles located inside fcc grains as well as at grain boundaries. The average grain size of the matrix is about $100 \text{ }\mu\text{m}$. A detailed EDS analysis reveals that the chemical composition (mass fraction) of fcc matrix is about 25.0% Fe, 23.1% Cr, 26.5% Ni and 25.5% Mn, while the composition of bcc phase is about 26.3% Fe, 37.4% Cr, 15.2% Ni and 21.2% Mn. The Cr-rich and Ni-Mn depleted bcc phase can be observed in Fig. 1a.

As shown in the boundary map of fcc phase in Fig. 1b, massive straight $\Sigma 3$ twin boundaries (denoted as red lines) exist in the matrix phase, while only a few low-angle grain boundaries (LAGBs, indicated by green lines) can be observed. Those twin boundaries form during the annealing process after forging, which is a general phenomenon for alloys with fcc crystal structure. Moreover, it has to be noted that the local misorientation value in the whole analysis area of the raw material is quite low, as shown in Fig. 1c. Since the local misorientation is directly connected with geometrically necessary dislocations, which are the result of local strain gradients, it can be used as a qualitative assessment of the dislocation density^[18,19]. The results indicate that the raw material possess a low dislocation density and no plastic deformation.

2.2 Flow curves

Typical true stress-true strain curves during hot compression of the duplex FeCrNiMn alloy at 950 and $1050 \text{ }^\circ\text{C}$ with strain rates of 0.1 and 0.01 s^{-1} are shown in Fig. 2. All the compression tests were finished until reaching a true strain of about 1. The flow curves show a linear decrease in the stress with increasing strain after reaching a maximum value, and the maximum stresses decrease with increasing temperature and decreasing strain rate, which is similar to the cases of other commercial alloys insofar. However, an interesting

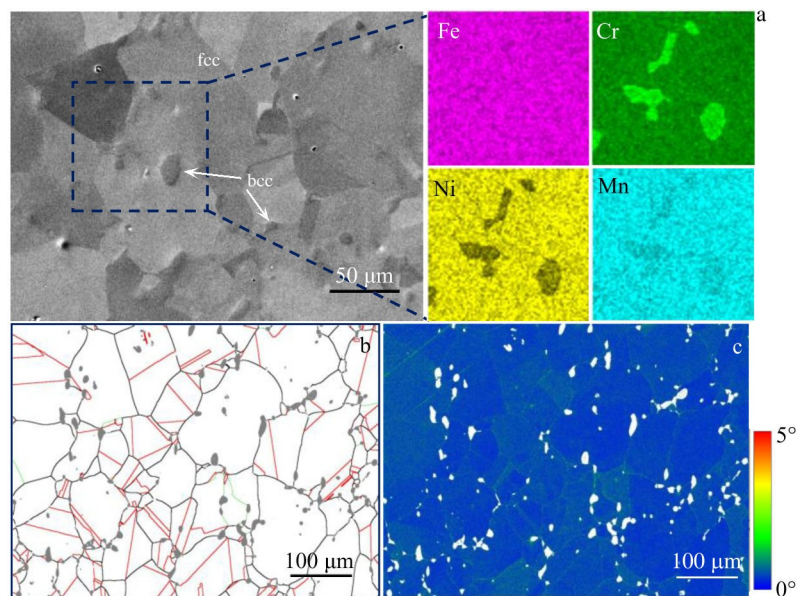


Fig.1 SEM image and EDS mapping of annealed FeCrNiMn alloy (a); boundary map of fcc phase, in which the green and black lines indicate boundaries with misorientations of $2^\circ < \theta < 15^\circ$ and $\theta > 15^\circ$, respectively, red lines denote $\Sigma 3$ twin boundaries and bcc phase is coloured in grey (b); local misorientation map of fcc phase in the same region (c)

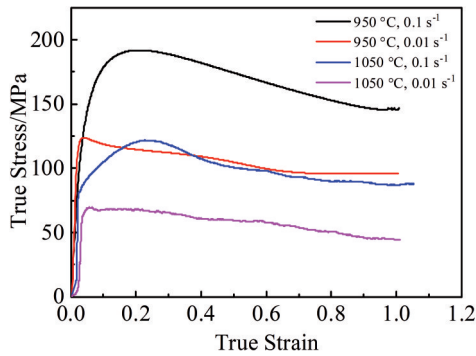


Fig.2 Typical true stress-true strain curves of FeCrNiMn duplex high entropy alloys compressed at 950 and 1050 °C with strain rates of 0.1 and 0.01 s⁻¹

difference in the flow curves is observed between different deformation conditions. The flow curves of the duplex FeCrNiMn alloy deformed at a strain rate of 0.1 s⁻¹ exhibit a typical type of DRX flow. It consists of a broad peak around the maximum stress. The compressive stress increases at the early stage until reaching the true strain of about 0.2, then it decreases gradually with increasing strain. Nevertheless, the flow curves obtained at the strain rate of 0.01 s⁻¹ are quite different: no steady state exists and a sharp softening arises immediately after reaching the maximum stress.

It has been investigated that different factors, including strain partitioning, texture softening, interphase sliding and distortion of coherent interphase boundaries, might influence the flow curves of duplex alloys^[20,21]. The flow curves of the duplex HEAs tested at different strain rates differ from each other, which should be attributed to the balance between the work-hardening and softening mechanisms. Thus, the

microstructure evolution during compression of the FeCrNiMn alloy is discussed in the next section.

2.3 Microstructure evolution during hot compression

2.3.1 Recrystallization of fcc phase

EBSD analysis results of fcc phases in the FeCrNiMn alloy compressed to a true strain of about 1 at 950 °C under strain rates of 0.1 and 0.01 s⁻¹ are presented in Fig. 3. In this and subsequent figures, the vertical direction corresponds to the compression direction (CD) of the samples. The scanning was performed under a step size of 0.5 μm for Fig. 3a, 3b, 3d, 3e and 0.15 μm for Fig. 3c, 3f. In the boundary maps, the orientation differences between neighboring grid points, including $2^\circ < \theta < 15^\circ$, $\theta > 15^\circ$ and $\theta = 60^\circ$, are marked by green, black and red lines, respectively, and bcc phase is coloured in grey.

As shown in Fig. 3a and 3d, the fcc grains are elongated along the direction perpendicular to CD and a large amount of recrystallized grains can be observed in the vicinity of original grain boundaries. Although some grains with large size are still retained after hot compression, the appearance of numerous DRX grains can reduce the average grain size. Fig. 3b and 3e show the distribution of grain boundaries under different deformation conditions. The densely distributed LAGBs inside fcc grains indicate a severe plastic deformation, which is similar to local misorientation. It shows that the plastic deformation is concentrated in the edge region of fcc grains, while only a few LAGBs can be observed in the central region. A detailed analysis was conducted with a step size of 0.15 μm and the results are shown in Fig. 3c and 3f. Two phenomena can be got from these figures: the DRX grains are accompanied by many twin boundaries; DRX tends to take place near grain boundaries, especially interphase boundaries. Comparing two different deformation conditions, it is found

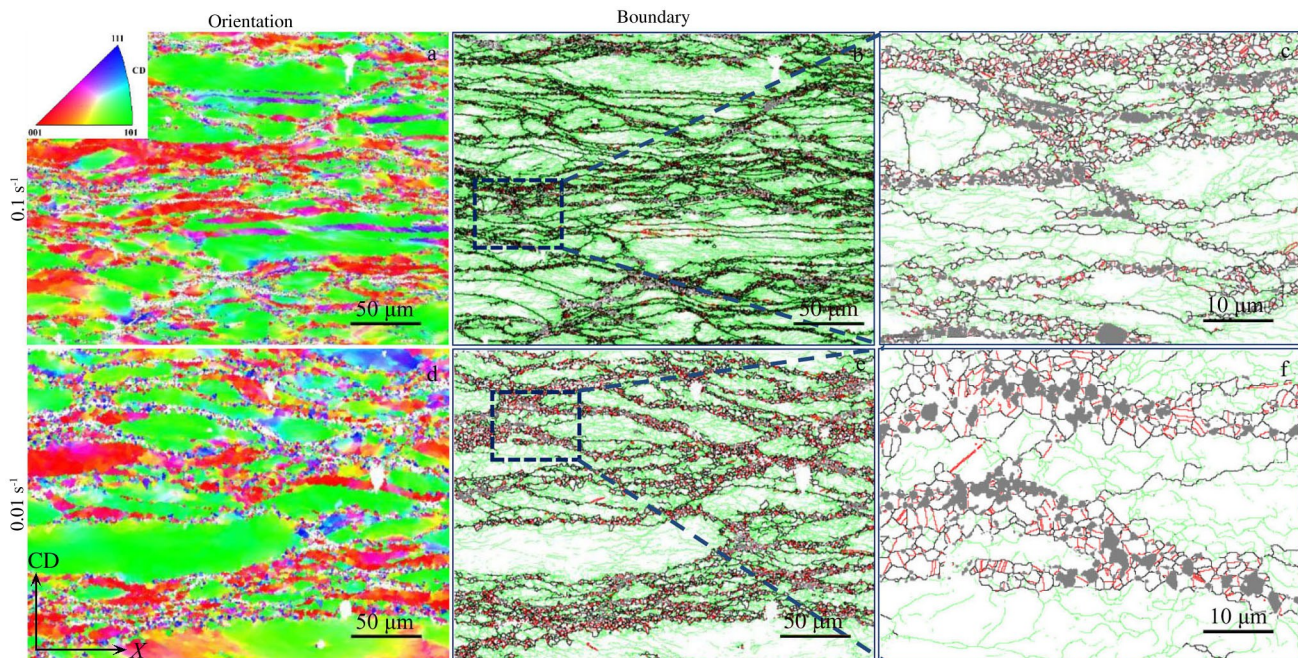


Fig.3 EBSD characteristics of fcc phase in the FeCrNiMn alloy compressed at 950 °C with strain rates of 0.1 s⁻¹ (a~c) and 0.01 s⁻¹ (d~f)

that the density of LAGBs is lower under the strain rate of 0.01 s^{-1} and the size of recrystallized grains is larger, which is attributed to the enhancement of DRX at a lower strain rate.

Fig. 4b displays the EBSD results of fcc phases in the FeCrNiMn alloy compressed at $1050 \text{ }^\circ\text{C}$. The microstructure evolution of the sample compressed at $1050 \text{ }^\circ\text{C}$ with a strain rate of 0.1 s^{-1} is similar to that of the sample deformed at $950 \text{ }^\circ\text{C}$. The fcc grains are elongated perpendicular to CD and a large amount of recrystallized grains can be observed in the vicinity of original grain boundaries, especially interphase boundaries. Meanwhile, a large amount of $\Sigma 3$ twin boundaries are generated in the DRX process. In contrast, equiaxed fcc grains with an average grain size of about $50 \text{ }\mu\text{m}$ are obtained after compression at $1050 \text{ }^\circ\text{C}$ under a strain rate of 0.01 s^{-1} . The twin boundaries are distributed evenly in fcc grains, and bcc particles are located at grain boundaries as well as inside fcc grains. Actually, the microstructure of the FeCrNiMn alloy after compression at $1050 \text{ }^\circ\text{C}$, 0.01 s^{-1} is nearly the same as the initial structure, except for a much smaller grain size.

It can be drawn from the above analysis that the DRX of duplex HEAs is strengthened at higher deformation temperature and lower strain rate. As has been investigated previously, two DRX nucleation mechanisms occur during the deformation of duplex alloys, including twinning and the formation of geometrically necessary boundaries^[22]. It depends on which mechanism dominates the DRX process under the deformation conditions. In this study, the main feature of the recrystallized regions is the presence of abundant $\Sigma 3$ twin boundaries, which reveal the occurrence of DRX followed by twinning in this alloy. It is reasonable to consider the low stacking fault energy of the fcc phase in the duplex FeCrNiMn alloy^[23]. Moreover, it has to be noted that recrystallization is concentrated in the vicinity of grain boundaries, especially interphase boundaries. Thus, bcc phase has an important effect

on the DRX during hot compression of duplex HEAs.

2.3.2 Texture evolution of fcc phase

The $\{111\}$, $\{110\}$ and $\{100\}$ (equal area projection) pole figures of fcc phase in the FeCrNiMn alloy compressed to a true strain of about 1 under different conditions are shown in Fig. 5. The structures analyzed here cover deformed, recovered and new DRX grains. It can be seen that a strong pole along the CD exists in the $\{110\}$ pole figures of Fig. 5a, which reveals a classical compression deformation texture consisting of a $\langle 110 \rangle$ fiber along the compression axis in the sample deformed at $950 \text{ }^\circ\text{C}$, 0.1 s^{-1} . As shown in Fig. 5b, the $\langle 110 \rangle$ fiber texture is weakened as the strain rate decreases to 0.01 s^{-1} . Compression at $1050 \text{ }^\circ\text{C}$ and 0.1 s^{-1} produces a two-component texture combining the $\langle 110 \rangle$ and $\langle 100 \rangle$ components (Fig. 5c). When the strain rate decreases to 0.01 s^{-1} , the texture structure disappears.

The $\{110\}$ fiber texture generated during the compression at 950 and $1050 \text{ }^\circ\text{C}$ at the strain rate of 0.1 s^{-1} is attributed to the polycrystal rotation during deformation such that most $\{110\}$ planes of fcc phase become perpendicular to the loading axis. It is similar to other commercial alloys with fcc crystal structure^[24,25]. The DRX process is accompanied with the generation of many new grains with random orientation. Thus, the texture is weakened and even totally eliminated as the strain rate decreases to 0.01 s^{-1} . In this study, it is interesting to note that a two-component texture combining the $\langle 110 \rangle$ and $\langle 100 \rangle$ components is produced at $1050 \text{ }^\circ\text{C}$, 0.1 s^{-1} , which can be attributed to the diffusion-controlled solute drag as the dominant deformation mechanism at higher temperatures, which is similar to the texture evolution of aluminum alloys.

2.3.3 bcc phase

Fig. 6 shows the characteristics of bcc phases in the FeCrNiMn alloy deformed at $950 \text{ }^\circ\text{C}$, 0.1 s^{-1} and $1050 \text{ }^\circ\text{C}$, 0.01 s^{-1} . According to the statistical analysis of EBSD results,

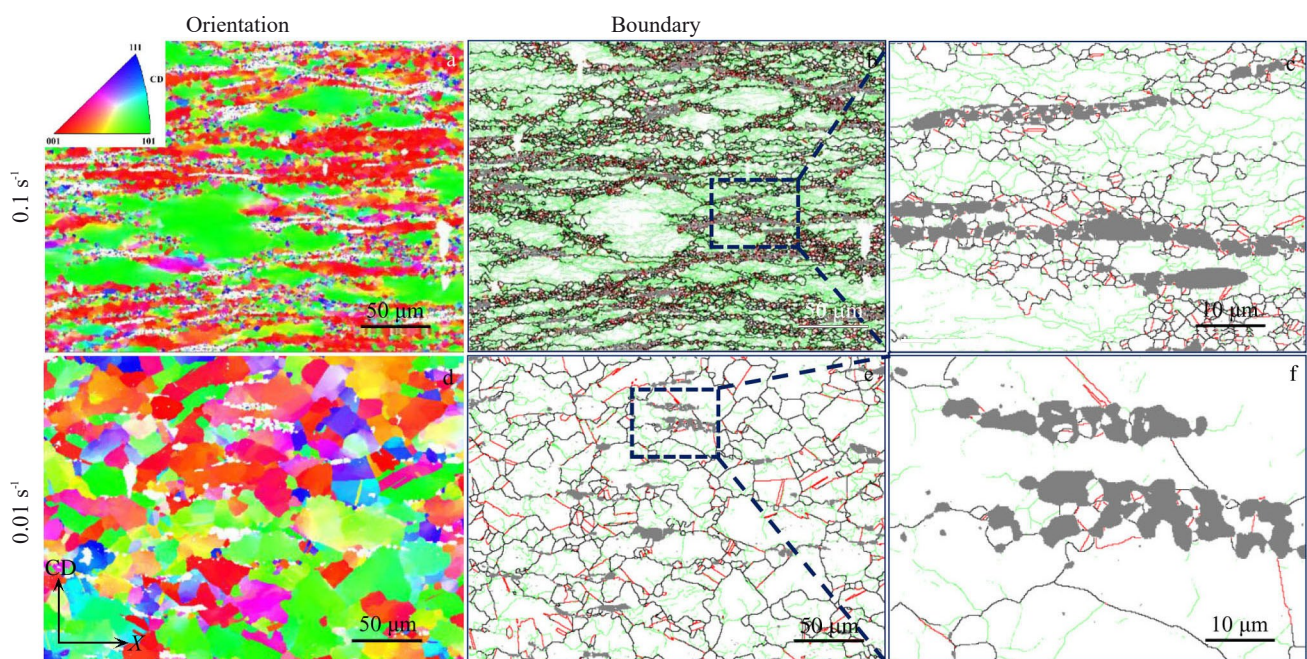


Fig.4 EBSD results of FeCrNiMn alloy compressed at $1050 \text{ }^\circ\text{C}$ with strain rates of 0.1 s^{-1} (a-c) and 0.01 s^{-1} (d-f)

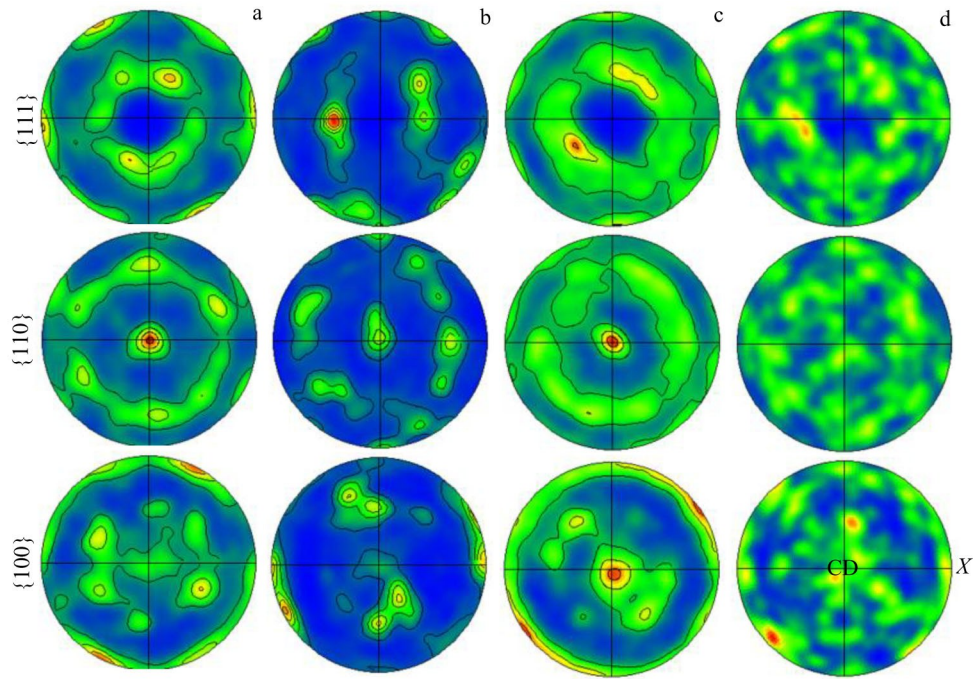


Fig.5 Pole figures of fcc phase in FeCrNiMn alloy compressed under different conditions: (a) 950 °C, 0.1 s⁻¹; (b) 950 °C, 0.01 s⁻¹; (c) 1050 °C, 0.1 s⁻¹; (d) 1050 °C, 0.01 s⁻¹

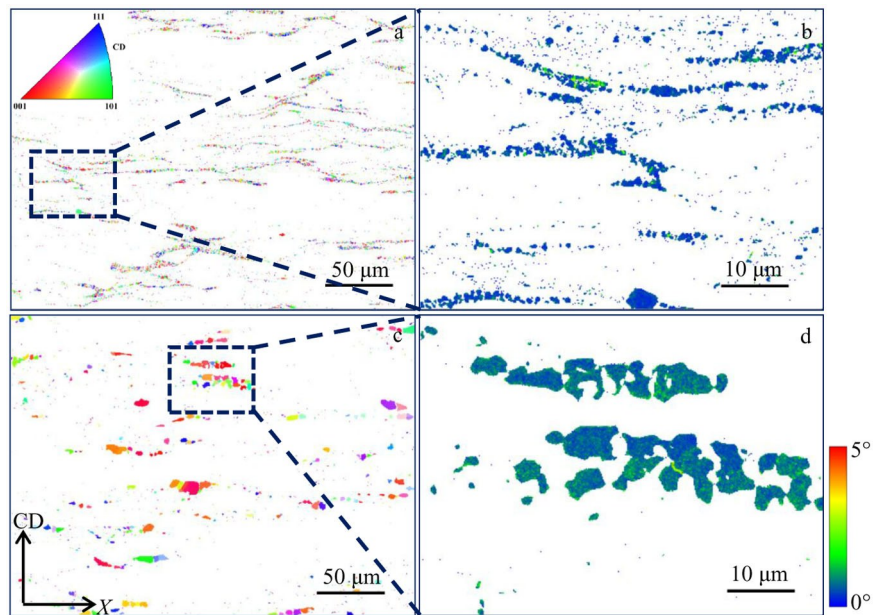


Fig.6 EBSD characteristics of bcc phase in FeCrNiMn alloy deformed under 950 °C/0.1 s⁻¹ (a, b) and 1050 °C/0.01 s⁻¹ (c, d): (a, c) orientation maps for CD colouring and (b, d) local misorientation maps

the volume fraction of bcc phase after compression under different conditions is all about 4%. It means that the annealed material is stable during compression and no phase transformation occurs. As shown in Fig.6a, fine bcc particles are distributed in band shape along the direction perpendicular to CD, which exhibit a random crystallographic orientation. After the compression at 1050 °C, 0.01 s⁻¹, the bcc particle size remains constant. However, it is also distributed in line

perpendicular to CD, as shown in Fig.6c. Additionally, the bcc particles are mostly strain-free after compression under two different conditions. As shown in Fig.6b and 6d, only a few particles with a relatively larger local misorientation can be found. Thus, most of the plastic strain is accommodated by softer fcc grains rather than bcc particles.

It has been indicated previously in Section 2.3.1 that bcc phase has an important effect on the DRX during hot

compression of duplex HEAs. The EBSD results show that no phase transformation occurs during compression and most of the strain is accommodated by fcc phase rather than bcc particles. Therefore, the effect of bcc phase on the DRX of duplex HEAs is attributed to interphase boundary and strain heterogeneity around these particles. The bcc particles only undergo fragmentation during hot compression. However, the interphase boundaries and strain heterogeneity possess an important influence on the DRX and mechanical behavior of duplex HEAs.

3 Conclusions

1) An obvious difference of the flow curves can be observed for the FeCrNiMn duplex alloy deformed at the strain rates of 0.1 and 0.01 s⁻¹.

2) The difference of mechanical flow curves can be correlated with the DRX and texture evolution process.

3) A two-component texture combining the <110> and <100> components can be obtained after compression at 1050 °C and 0.1 s⁻¹, which is attributed to the diffusion-controlled solute drag at higher temperatures.

4) The effect of bcc phase during compression of duplex HEAs is dependant on interphase boundary and strain heterogeneity around these particles, since no phase transformation occurs and most of the strain is accommodated by fcc phase.

References

- 1 Yeh J W, Chen S K, Lin S J et al. *Advanced Engineering Materials*[J], 2004, 6: 299
- 2 Zhang Y, Zuo T T, Tang Z et al. *Progress in Materials Science*[J], 2014, 61: 1
- 3 Miracle D B, Senkov O N. *Acta Materialia*[J], 2017, 122: 448
- 4 Pickering E J, Jones N G. *International Materials Reviews*[J], 2016, 61: 183
- 5 Yeh J W. *Annales De Chimie-Science Des Materiaux*[J], 2006, 31: 633
- 6 Hsu C Y, Yeh J W, Chen S K et al. *Metallurgical and Materials Transactions A*[J], 2004, 35: 1465
- 7 Roksolana K, Alla S, Walter S. *Zeitschrift für Kristallographie-Crystalline Materials*[J], 2015, 230: 55
- 8 Couzinié J P, Dirras G. *Materials Characterization*[J], 2019, 147: 533
- 9 Li Z, Zhao S, Ritchie R O et al. *Progress in Materials Science* [J], 2019, 102: 296
- 10 Ye Y F, Wang Q, Lu J et al. *Materials Today*[J], 2016, 19: 349
- 11 George E P, Curtin W A, Tasan C C. *Acta Materialia*[J], 2020, 188: 435
- 12 Tsai C W, Chen Y L, Tsai M H et al. *Journal of Alloys and Compounds*[J], 2009, 486: 427
- 13 Gourdet S, Montheillet F. *Acta Materialia*[J], 2003, 51: 2685
- 14 Lee K S, Bae B, Kang J H et al. *Materials Letters*[J], 2017, 198: 81
- 15 Kim W J, Jeong H T, Park H K et al. *Journal of Alloys and Compounds*[J], 2019, 802: 152
- 16 Haghdad N, Primig S, Annasamy M et al. *Journal of Alloys and Compounds*[J], 2020, 830: 154 720
- 17 Annasamy M, Haghdad N, Taylor A et al. *Materials Science and Engineering A*[J], 2019, 745: 90
- 18 Wang Y M, Voisin T, McKeown J T et al. *Nature Materials*[J], 2017, 17(1): 63
- 19 Shen R R, Ström V, Efsing P. *Materials Science & Engineering A*[J], 2016, 674: 171
- 20 Iza-Mendia A, Pinol-Juez A, Urcola J J et al. *Metallurgical & Materials Transactions A*[J], 1998, 29: 2975
- 21 Sun B, Aydin H, Fazeli F et al. *Metallurgical & Materials Transactions A*[J], 2016, 47: 1782
- 22 Wusatowska-Sarnek A M, Miura H, Sakai T. *Materials Science and Engineering A*[J], 2002, 323: 177
- 23 Pei Z. *Materials Science and Engineering A*[J], 2018, 737: 132
- 24 Bronkhorst C A, Kalidindi S R, Anand L. *Philosophical Transactions: Physical Sciences & Engineering*[J], 1992, 341: 443
- 25 Hughes D A, Kassner M E, Stout M G et al. *Journal of Metals*[J], 1998, 50: 16

FeCrNiMn 双相高熵合金高温压缩过程中的组织演变

梅金娜¹, 吴天栋^{2,3}, 卫娜^{2,3}, 蔡振¹, 薛祥义^{2,3}

(1. 苏州热工研究院有限公司, 江苏 苏州 215004)

(2. 西安超晶科技股份有限公司, 陕西 西安 710200)

(3. 陕西省先进金属结构材料精确热成形重点实验室, 陕西 西安 710200)

摘要: 为了研究双相高熵合金 (HEA) 在高温变形过程中的微观组织演变, 在 900 至 1050 °C 的温度下进行了不同应变速率的压缩试验。选择了 4 种典型的流动曲线, 并对相应的微观组织进行了分析, 以研究双相 HEA 的动态再结晶 (DRX) 和组织演变。结果表明, 在应变速率为 0.1 和 0.01 s⁻¹ 时, 变形试样的流动曲线完全不同。力学流动曲线的差异与 DRX 和组织演化过程有关。在 1050 °C 和 0.1 s⁻¹ 下压缩后, 获得了结合 <110> 和 <100> 的双组份组织结构, 这是因为高温下扩散控制的溶质阻力占主导地位。此外, bcc 相的影响依赖于界面边界和颗粒周围的应变不均匀性, 因为没有发生相变, 大部分应变由 fcc 相容纳。

关键词: 高熵合金; 组织演变; 高温变形; 流变曲线

作者简介: 梅金娜, 女, 1981 年生, 高级工程师, 苏州热工研究院有限公司, 江苏 苏州 215004, 电话: 029-86066135, E-mail: meijinna@cgnfc.com.cn